Cent. Eur. J. Phys. • 9(2) • 2011 • 530-541
DOI: 10.2478/s11534-010-0079-8

VERSITA

Central European Journal of **Physics**

Simulations on the mechanism of CNT bundle growth upon smooth and nanostructured Ni as well as θ-Al_2O_3 catalysts*

Research Article

Yuri F. Zhukovskii[1†], Sergei Piskunov[2,3‡], Eugene A. Kotomin[1§], Stefano Bellucci[4¶]

1 *Institute of Solid State Physics, University of Latvia, 8 Kengaraga Str., Riga LV-1063, Latvia*

2 *Faculty of Computing, University of Latvia, 19 Raina blvd., Riga LV-1586, Latvia*

3 *Faculty of Physics and Mathematics, University of Latvia, 8 Zellu Str., Riga LV-1002, Latvia*

4 *INFN-Laboratori Nazionali di Frascati, Via Enrico Fermi 40, Frascati, Italy*

Received 23 June 2010; accepted 31 August 2010

Abstract: In the current study, we have performed *ab initio* DFT calculations on the gradually growing 2D periodic models of capped single-wall carbon nanotubes (SW CNTs) upon their perpendicular junctions with the Ni(111) substrate, in order to understand the peculiarities of the initial stage of their growth on either smooth or nanostructured catalytic particles. Appearance of the adsorbed carbon atoms upon the substrate follows from the dissociation of CVD hydrocarbon molecules, *e.g.*, CH_4: $(CH_4)_{ads} \rightarrow (CH)_{ads}+3H_{ads}$ and $(CH)_{ads} \rightarrow C_{ads}+H_{ads}$. (Since the effective growth of CNTs upon Ni nanoparticles occur inside the nanopores of amorphous alumina, we have also simulated analogous surface reactions upon the θ-Al_2O_3(010) slabs). Association of the adsorbed carbon atoms upon the catalyst surface precedes further swelling of the $(C_n)_{ads}$ islands after appearance of pentagonal defects within a honeycomb sheet which are more probable upon the catalyst surface containing either defects or nanoclusters (as in the case of the nanostructured substrate). The gradual growth of the capped CNTs is considerably more effective upon the nanostructured Ni(111) substrate compared to a smooth nickel substrate (*cf.* values of CNT adhesion energy *per* boundary C atom for chiralities of either armchair-type, 4.04 *vs*. 2.51 eV, or zigzag-type, 4.61 *vs*. 2.14 eV, respectively). The electronic charge transfer from the Ni catalyst towards the CNTs has been calculated for both chiralities ($>$ 1 *e per* C atom), *i.e.*, quite strong chemical bonds are formed within the CNT/Ni(111) interconnects.

PACS (2008): 61.48.-c, 68.43.Bc, 68.47.-b, 68.55.A-, 71.15.-m, 73.63.Rt

Keywords: DFT calculations • flat and nanostructured surfaces of Ni and θ-Al_2O_3 catalysts • adsorption and dissociation of CH_4 • mechanism of CNT growth • bundles of single-wall CNTs • arcmchair and zigzag-type chiralities • CNT-Ni junction

*presented at the 6th International Conference on Functional Materials and Nanotechnologies, March 17-19, 2010, Riga, Latvia

†E-mail: quantzh@latnet.lv (Corresponding author)
‡E-mail: piskunov@lanet.lv
§E-mail: kotomin@latnet.lv
¶E-mail: Stefano.Bellucci@lnf.infn.it

1. Introduction

Due to their unique properties, carbon nanotubes (CNTs) become an important constituent for future generation nanoelectronics [1]. The progress in this field is still hindered by the inability to reproduce growth of CNTs with predetermined chirality indices (and thus the electronic properties) since the contemporary methods of nanotube synthesis yield a mixture of metallic and semiconducting nanotubes with varying band gaps. The chemical vapor deposition (CVD) growth of CNTs above the particles of a metallic catalyst positioned inside the alumina membrane (on the bottom of its semi-closed nanopores) is believed to be the most promising approach for gaining control over the geometry and the electronic properties of nanotubes [2]. Moreover, the CVD growth of nanotubes can be achieved at low temperature, which is another important requirement for application of CNTs in nanoelectronics. The structure of interconnections between the metallic catalyst nanoparticle and the CNT is important for understanding both the electronic transport through the nanotube and the mechanism of its growth. Decomposition of gas-phase carbon-hydrogen precursors (C_nH_m) on the catalyst surface is the first step for the CVD growth of CNTs. This initial step is followed by two important processes: (*i*) the diffusion of carbon on the particle surface or across its interior (a rate-determining step) and (*ii*) the nucleation of the graphitic fragment as followed by further incorporation of carbon into the growing nanotube which determines CNT chirality [3]. Depending on the size and the structure of such a catalyst particle, either the well-separated single-wall (SW) nanotubes and their bundles (containing up to several hundred of the closely-packed nanotubes of different chiralities) or MW (multi-wall) NTs, whose shells possess various chiralities, could be synthesized. The microscopic images of CNTs growing upon the catalytic nanoparticles [4] help to clarify how the models of the Me-CNT junction can be drawn. The optimal performance of carbon nanotubes requires control of their structural properties [5], *e.g.*, size, length, chirality, which remains a significant difficulty for the widespread application of CNTs in high-technology devices.

The formation of SW CNTs mainly requires the presence of transition-metal element or alloy catalysts (Co, Ni, Fe, Y, *etc.* [6–8]). Both separated nanotubes and their bundles were synthesized *via* the interaction of metal catalyst nanoparticles with carbon or hydrocarbon vapor at relatively high temperature. These catalysts are crucial for the controlled synthesis of SW CNTs by such a technique as CVD [9–11]. However, the exact role played by the metal atoms in the growth of SW CNTs is still under study [12]. Within solid solutions or ordered compounds, the metal-C bonds are predominant around carbon atoms. When phase separation occurs, C atoms can form either pure graphite or well-crystallized carbon phases whose atoms form covalent sp^3-, sp^2- or even *sp*- bonds. The catalytic growth of SW CNT involves segregation and diffusion processes of carbon adatoms and their self-organization into islands with the structure of graphene sheets and fullerene-like nanotube embryos positioned upon the catalytic surface [13]. The swelling of graphene-like islands towards semi-fullerene embryos was found to be possible after creation of pentagonal defects within a honeycomb structure which is more probable on a catalyst surface containing the structural irregularities, *e.g.*, nanoclusters.

Formation of graphene-like islands upon the substrate, their transformation to semi-fullerenes and further CNT growth can be simulated using the classical methods of molecular dynamics or mechanics for systems containing thousands of atoms [14]. On the other hand, application of simple phenomenological potentials is rather problematic since such potentials can hardly account for the quantum nature of the different types of covalent bonds in the CNT/Me atomistic model. From this point of view, the first principle electronic structure calculations performed recently for simulation of CNT growth upon various metal nanoclusters (Me = Ag, Au, Co, Cu, Fe, Ni, Pd, Pt) [5, 15–17], where the most likely armchair (m, m) and zigzag-type $(n, 0)$ chiralities were considered, look a more reliable alternative to various empirical potential simulations although quite complex dynamic and thermodynamic processes cannot be properly described. Thus, a combination of various methods for theoretical simulations could be more productive.

One of the effective theoretical approaches widely used for the qualitative understanding of reasons favorable to CNT growth upon the catalytic particle was found to be its thermodynamic description based on results of preliminary *ab initio* calculations [16]. The relevant diffusion channels of carbon adatoms on metallic and oxide substrates are addressed through the calculation of their activation barriers. For monoatomic carbon, all diffusion modes can be considered (surface, subsurface and bulk) while in the case of a carbon dimer, only the surface diffusion mode is usually studied. For the C adatom diffusion on the (111) face of a Ni nanocluster, a barrier of ~ 0.4 eV was obtained [18], in agreement with the measured activation energy of the experimental CNT growth process, suggesting that surface diffusion is the rate-limiting step [4]. Subsurface and bulk diffusion occur *via* hopping of interstitial carbon atoms between adjacent tetrahedral and octahedral voids which is generally higher than for adatom diffusion. However, the activation energy for the subsurface diffusion decreases with the increasing lattice constant, following an opposite

trend with respect to the adatom diffusion and leading to competition between the two diffusion modes. Activation barriers of subsurface diffusion are always lower than those of corresponding bulk diffusion due to the reduced elastic response in the proximity of the nanocluster surface.

To understand the relation between the chirality of growing CNTs and the chemical composition of catalyst, a comprehensive study of the interaction between the graphitic fragments and the metallic nanoparticles is required [19]. Clearly such a study is computationally expensive because of the large configuration space involved. To address this issue, one can focus on the binding of minimal structural units of armchair (*ac*) and zigzag (*zz*) edges to either flat or stepped surfaces. The binding energies are quantified by the chemical potential *per* edge atom μ_{edge} defined as [16]:

$$\mu_{edge} = \mu_{edge}^{free} + \frac{E - E_{Ni} - E_{frag}}{n_C}, \qquad (1)$$

where μ_{edge}^{free} is the chemical potential *per* edge atom for an unbound edge, E and E_{Ni} are the total energies of the Ni substrate with and without carbon, respectively, E_{frag} the total energy of an isolated model fragment and n_C the number of edge C atoms. The value of μ_{edge}^{free} can be estimated through the calculations of ideal graphene monolayers and suitable graphene nanoribbons (GNRs).

The calculated chemical potentials corresponding to optimally placed fragments bound to facets or step edges are always lower than those of separated adatoms, *i.e.*, an aggregation of C atoms is energetically favored. Moreover, $\mu_{edge} > 0$, which means that a certain driving force exists towards the extending graphitic fragments, *e.g.*, CNTs. The combination of these features points to the existence of a negative chemical potential gradient for the nucleation and further growth of CNTs from a carbon feedstock. Analysis of the chemical potentials can also explain the ability of catalysts for growth of CNTs with definite chiralities. For metals, *e.g.*, Ni, *ac*-edges were found to be more stable than *zz*-edges. For a quantitative measure of this preference at growth temperature T, the following ratio was presented [16]:

$$R^T = \exp\left[-\frac{\mu_{edge}^{ac} - \mu_{edge}^{zz}}{kT}\right], \qquad (2)$$

assuming that the CNT nucleation occurs under thermodynamic control. For nanotube embryos, the chemical potential of the edge carbon atoms is higher than that of other C atoms, thus, leading to the growth of CNT with minimum edge perimeters. It means that R^T characterizes the distribution of nanotube chiralities indicating the preference for growth of either *zz*- or *ac*-like nanotubes. Ultimate selectivity is achieved for *zz*- and *ac*-CNTs, at $R^T = 0$ and $R^T \to \infty$, respectively. All metals show a strong preference for growing *ac*- rather than *zz*-nanotubes, in agreement with the experimental data obtained for Fe-group transition metals [20].

When applying CVD processes the SW CNT grow in a tangential mode, with the nanotube diameter being related to the size of the catalyst particle. In other cases, particularly in high-temperature synthesis, the nanotubes grow perpendicularly to the surface [8]. Several arguments based on classical nucleation and growth thermodynamic models have been put forward to understand how this can happen [21, 22]. C adatoms at the catalyst surface are assumed to condense in the form of graphene flakes. Then the metallic substrate can assist to saturate the dangling bonds which favor the formation of a cap, with the energy cost due to the curvature induced by the presence of pentagons being more than compensated by the reduction in the number of dangling bonds. Earlier this model was partly confirmed [23] when *ab initio* energy calculations of different carbon atom arrangements on a Ni substrate were performed. When carbon atom aggregates curve to form caps, the energy gain becomes concentrated on the carbon and nickel atoms close to their edge [5], i.e., one might argue that the dangling bonds are saturated, however, this is a weak effect which does not play an exclusive role in favor of curved caps. At least for small metal clusters, the adhesion energies of flat and curved sheets are similar and small compared to dangling-bond energies.

In the current study, we have performed a series of DFT (Density Functional Theory) calculations on 2D periodic models of carbon-containing adsorbate upon smooth or nano-structured Ni(111) substrates, varying from the CH_4 molecules up to the gradually growing bundles of capped SW CNTs possessing either *ac*- or *zz*-type chirality. This periodic model is limited since nanotube chiralities and sizes in bundles are set equivalent (although really synthesized bundles contain CNTs of different morphology) while the inter-shell distances (0.42-0.46 nm) are overestimated as compared to those experimentally observed in CNT bundles (0.34 nm). Since our study is focused on the development of models describing the growth mechanism of CNTs inside the pores of amorphous alumina membranes, we have also estimated possibilities for CNT growth upon the θ-Al_2O_3(010) substrate structurally close to amorphous alumina. The paper is organized as follows: Section 2 deals with the computational details. Models of different configurations for both C/Ni and C/θ-Al_2O_3 interfaces as well as properties calculated for them are discussed and compared in Section 3, while Section 4 presents main conclusions.

2. Computational details

The first-principles DFT-LCAO method (Linear Combination of Atomic Orbitals), as implemented in the *CRYSTAL-06* code[1], allows us to describe both 1D nanotubes and 2D sheets in their original space form, unlike the Plane-Wave (PW) methods which are quite widespread nowadays for *ab initio* calculations on low-dimensional periodic systems, including CNT-Me interconnects [15–17]. Indeed, to restore the 3D periodicity in the PW nanotube calculations, the $x-y$ supercell of nanotubes is artificially introduced: The NTs are placed into a square array with the inter-tube distance equal to 1-3 nm. At such separations the NT-NT interaction is usually found to be rather small, however, the convergence of results obtained using such PW calculations depends on the artificial inter-tube interactions, thus, the additional computational efforts should be provided to ensure their negligibility. Analogous problems also appear in PW calculations on the 3D slab models. Such an artifact is certainly absent when using LCAO formalism for description of nanotubes and slabs.

Our calculations have been performed for all configurations of carbon-containing adsorbate above the Ni or θ-alumina substrates as described in Section 3. The crystalline orbitals $\varphi_{ki}(\mathbf{r})$ of the N-electron system (*per* unit cell), according to the LCAO approach, are expanded as linear combinations of a set of m Bloch functions built from the local, atom-centered Gaussian-type functions (GTFs):

$$\varphi_{ki}(\mathbf{r}) = N\sum_{j=1}^{m} a_{ij}(\mathbf{k})\left(\sum_{\mathbf{g}} \chi_{gj}(\mathbf{r})\exp(\mathrm{i}\mathbf{k}\cdot\mathbf{g})\right), \qquad (3a)$$

$$\chi_{gj}(\mathbf{r}-\mathbf{R}_j) = \sum_{\mu}^{n_G} c_\mu G(\alpha_\mu;\mathbf{r}-\mathbf{R}_j-\mathbf{g}), \qquad (3b)$$

where $\mathbf{k}$ is the wave vector of the irreducible representation of the group of crystal translations $\{\mathbf{g}\}$; $\mathbf{R}_j$ denotes the coordinates of nuclei in the zero cell of which the atomic orbital $\chi_{gj}(\mathbf{r})$ is centered; G, c_μ and α_μ are the normalized GTFs, its coefficients and exponents, respectively. Earlier, this LCAO formalism was successfully applied by us for simulations on: (*i*) smooth and nanostructured Ni(111) substrates [24], (*ii*) α-Al_2O_3(0001) surface [25], (*iii*) SW nanotubes of AlN [26] and BN [27]. In the current study, we have used the all-valence basis sets (BSs) of atomic GTFs (constructed using pure *s*- and *d*- as well as hybrid *sp*-AOs)[1] as described elsewhere: Ni (8*s*-64111*sp*-41*d*) [24], Al (8*s*-621*sp*-1*d*) [26] and O (8*s*-411*sp*-1*d*) [27] which have been slightly re-optimized for valence and virtual shells. The BS of C atom in the suggested form (6*s*-311*sp*-11*d*)[1] have also been re-optimized. The gradient-corrected (GGA) exchange-correlation DFT functional by Perdew, Burke and Ernzerhof (PBE) [28] has been used in our spin-polarized calculations. To provide a balanced summation in both direct and reciprocal lattices, the reciprocal space integration has been performed by sampling the Brillouin zone with the $2\times2\times1$ Pack-Monkhorst mesh [29], which results in 2 k-points in total for 5×5 surface supercell of Ni(111) and unit cell of θ-Al_2O_3(010) slab models (Figs. 1 and 2 respectively). Calculations are considered as converged only when the total energy differs by less than 10^{-7} a.u. in two successive cycles of the self-consistency procedure. A smearing temperature of 0.001 a.u. applied to the Fermi function has been chosen relatively low, to ensure that the magnetic moment is not artificially modified by a too high value. All the calculations have been performed with total geometry optimization.

[1] R. Dovesi et al., CRYSTAL06 User's Manual (University of Torino, Turin, 2006), http://www.crystal.unito.it/

3. Results and discussion

In this Section, we compare and verify the results of our *ab initio* simulations performed on 2D periodic models, which describe peculiarities of the initial stage of growth for the bundle of SW CNTs upon the catalyst particle. The only limitation of this 2D model is that both the chirality and diameter of CNTs in the bundle are equivalent. This is a first attempt undertaken to simulate the periodic distribution of carbon nanotubes grown upon the catalyst surface in the framework of 2D-periodic model.

3.1. Models of nickel and alumina catalytic substrates

As a first stage for these simulations, we consider 2D adsorbate-less models of both smooth and nanostructured Ni(111) surfaces as well as θ-Al_2O_3(010) substrate (Figs. 1 and 2 respectively). The supercell (SC) of a smooth nickel (111) slab shown in Fig. 1a has been constructed from cubic *fcc* Ni crystal (space group *Fm3m*, the lattice constant 3.532 Å, $\alpha=\beta=\gamma=90°$), 5-layer slab contains 125 atoms *per* SC. The nanostructured Ni(111) surface contains a pyramid-like cluster *per* 5×5 supercell atop the smooth (111) surface (Figs. 1b, 1c) which includes seven and three nickel atoms in the corresponding sites of the 1st and 2nd (111) sublayers, respectively. Properties of smooth and nanostructured Ni(111) surfaces were simulated in our previous paper [24].

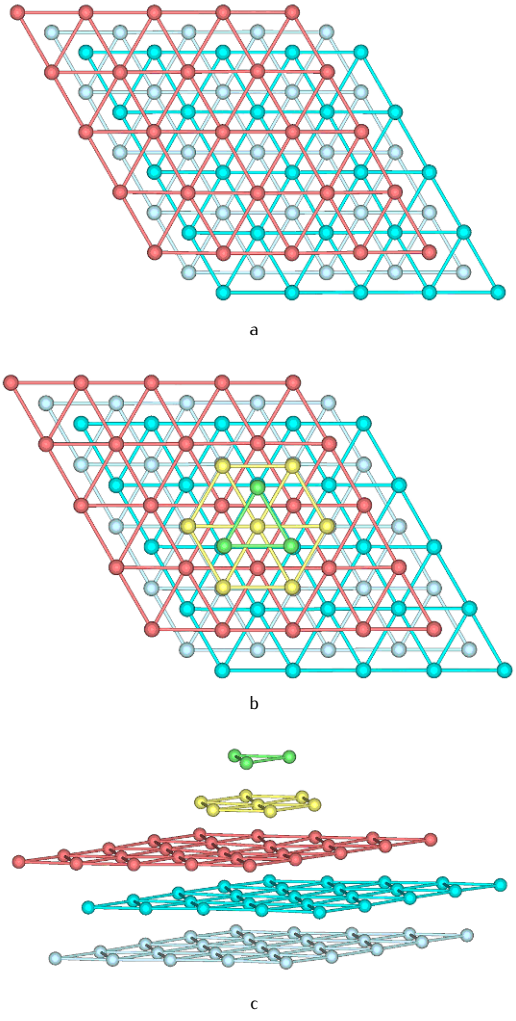

Figure 1. Images of smooth Ni(111) surface supercell (a) and that containing 10-atom Ni nanocluster upon the surface: top (b) and side (c) views. Each surface plane of nanostructured model is shown by a different color (grayscale halftones). The lower (light-blue) plane either coincides with a central layer of 5-layer slab or it is one of surface plane in 3-layer slab.

The model of θ-alumina surface has been chosen in the current study since it is thermally the most stable transition phase of alumina used in many high-temperature applications [30]. Moreover, its structure is less-ordered as compared to other alumina crystalline phases being structurally closer to amorphous Al_2O_3 [31]. The unit cell (UC) of a 7-layer θ-Al_2O_3(010) slab containing 70 atoms *per* UC (Fig. 2) has been cut from a monoclinic lattice of θ-alumina (space group $C2/m$, the lattice constants $a = 11.795$ Å, $b = 2.91$ Å, $c = 5.621$ Å, $\alpha = \gamma = 90°$, $\beta = 103.79°$).

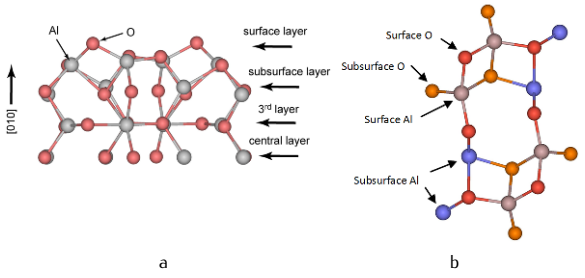

Figure 2. Images of 7-layer unit cell of symmetrically terminated θ-Al_2O_3(010) slab: side view (a) and top view (b). The arrows show planes perpendicular to surface and parallel to it.

3.2. Models of CH_4 molecule dissociation upon Ni and θ-Al_2O_3

The network of the adsorbed carbon atoms, which then transforms to CNT structures, can arise after the dissociation of hydrocarbon molecules, *e.g.*, the simplest CH_4 (point group T_d, equilibrium length of C-H bond 1.086 Å [32]), flowing towards the substrate when using the CVD method [2]. We estimate the dissociation energies for CH_4 molecules (E_{diss}) on both substrates (see Fig. 2 for details) according to the total energy balance of the two-step dissociation mechanism:

$$(CH_4)_{ads} \rightarrow (CH)_{ads} + 3H_{ads}, \tag{4a}$$

$$(CH)_{ads} \rightarrow C_{ads} + H_{ads}. \tag{4b}$$

The energetically most preferable site for adsorption of the methane molecule on the Ni substrate has been found to be the hollow *fcc* site, due to orientation compatibility between CH_4 molecule and both the smooth and nanostructured Ni(111) surface (Fig. 3) while upon the θ-Al_2O_3(010) substrate it is a bridge site on the Al-O bond.

The calculated values of initial binding energy (E_{ads}) *per* CH_4 molecule on the adsorbent sites shown in Fig. 3 have been estimated to be 1.00 eV (for both a smooth and nanostructured Ni substrate) *vs.* 0.25 eV (for θ-alumina surface). Comparison of the total dissociation energies of the CH_4 molecule upon the same sites clearly shows that the presence of small periodically distributed polyhedral

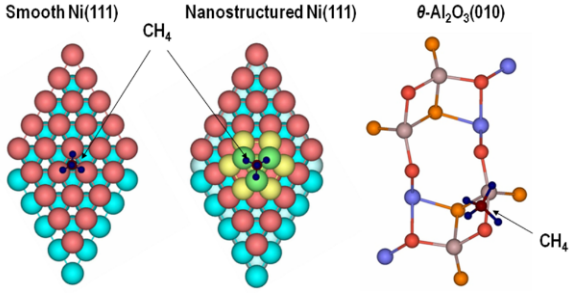

Figure 3. Images of models for CH_4 molecule dissociation upon both Ni(111) and θ-Al_2O_3(010) substrates.

nanoclusters (Fig. 3) results in preferable carbon atomization. The calculated energies of a complete dissociation (E_{diss}) have been found to be 2.33 eV and 2.17 eV *vs.* 4.87 eV respectively. It clearly indicates that the presence of edges on the Ni particle relieves carbon atom association and further CNT growth. On the other hand, the high energy barrier for complete dissociation of hydrocarbon molecules on the θ-Al_2O_3(010) surface results rather in CH_x-group appearance which can easy form hydrogen bonds with an alumina substrate. It means that alumina being a good catalyst for many chemical processes is noticeably less preferable for the growth of carbon nanotubes than transition metal catalysts. Detailed analysis of possibilities for CNT growth can be performed based on association of carbon atoms.

3.3. Models of single C atom adsorption upon Ni and θ-Al_2O_3

The binding energies of the newly-formed C_{ads} atoms on the smooth and nanostructured Ni(111) as well as θ-Al_2O_3(010) surfaces have been calculated using the following equation:

$$E_{bind} = -\frac{E_{complex} - E_{slab} - n_C E_C}{n_C}, \qquad (5)$$

where $E_{complex}$ is the calculated total energy of the slab with the attached C_n adsorbate, E_{slab} the total energy of the bare slab, E_C the energy of a single carbon atom in its ground state and n_C is the number of carbon atoms *per* supercell. The corresponding models are present in Figs. 4a, 4b.

Using Eq. (5) we could estimate the binding energies of carbon atoms upon different substrates and make conclusions on their ability to form carbon nanotubes (Tables 1, 2).

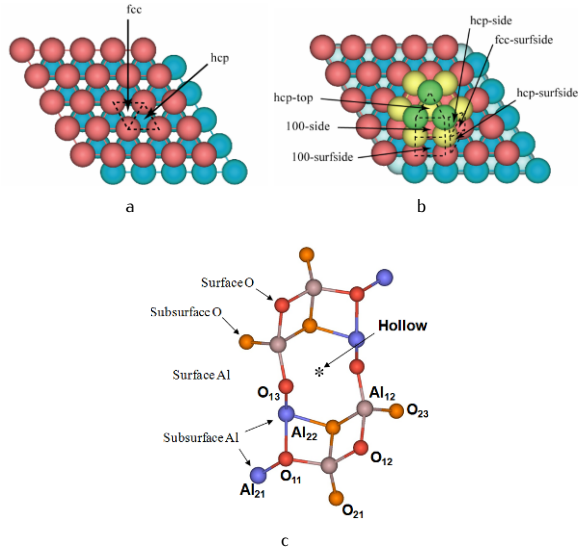

Figure 4. Images of models for single C atom adsorption molecule upon both Ni(111) (a,b) and θ-Al_2O_3(010) (c) substrates. In a) and b) red (dark gray) balls correspond to Ni atoms of surface layer, while blue (light gray) ones are for Ni atoms of subsurface layer.

Table 1. Calculated binding energies *per* single carbon adatom on smooth and nanostructured Ni(111) catalyst.

Structure:	E_{bind}, eV
hcp-Ni(111) (Fig. 4a)	7.09
fcc-Ni(111) (Fig. 4a)	6.39
hcp-top-nano-Ni(111) (Fig. 4b)	7.13
100-side-nano-Ni(111) (Fig. 4b)	8.08
100-surfside-nano-Ni(111) (Fig. 4b)	7.19
hcp-side-nano-Ni(111) (Fig. 4b)	6.93
fcc-surfside-nano-Ni(111) (Fig. 4b)	7.19
hcp-surfside-nano-Ni(111) (Fig. 4b)	7.48

The energetically most stable adsorption positions for a carbon atom with E_{bind} of $\sim$ 8 eV are aside (100) sites at nanostructured Ni(111) (Table 1), while θ-Al_2O_3(010) provides analogous adsorption sites with E_{bind} of maximum 2 eV (Table 2), *i.e.*, substantially smaller energy than that for the nickel substrate. As a result of our simulations, we predict an increase of catalytic activity of nanostructured Ni(111) surface due to nanofacet formation that potentially can play a role in a predictable growth of CNT.

Table 2. Calculated binding energies per single carbon atom adsorbed upon θ-Al_2O_3(010) (Fig. 4c).

Adsorbate position:	E_{bind}, eV
Al_{21}	1.34
O_{11}	1.09
Al_{11}	1.77
O_{21}	0.90
O_{12}	0.93
Al_{22}	0.65
O_{22}	2.03
Al_{12}	1.38
O_{23}	1.06
O_{13}	0.87
Hollow	0.60

3.4. Models of association of C atoms upon Ni substrates

After adsorption of single C atoms we have considered their further association. In our model of regular adsorption of carbon atoms atop the more preferable *hcp* sites on a smooth Ni(111) surface (Table 1) E_{bind} *per* C atom has been found to be 5.48 eV, *i.e.*, noticeably smaller than E_{bind} for a single adatom on the same site (7.09 eV) (*vs.* experimental value 6.9 eV [33]). This difference can be caused by a strong lateral interaction between adatoms. Translation vectors for such a regular C adsorbate structure have length 2.47 Å which is structurally compatible with the (111) face of adsorbent (length of analogous vector on nickel substrate is 2.49 Å), *i.e.*, their mismatch is ~0.8 per cent. To form the quasi-graphene structure, the neighboring C adatoms can be positioned above the neighboring *fcc*- and *hcp*-adsorption sites (Fig. 4a), *i.e.*, packing of adatoms must be double the case of regular adsorption upon the same type of surface sites. To form semi-fullerene-like embryos from quasi-graphene islands upon the surface of a nickel catalyst, they must contain pentagons which result in swelling of the islands and further growth of fullerene-like structures [34]. We consider this process on a smooth Ni(111) substrate when gradually increasing the number of C adatoms.

The values of binding energies presented in Figs. 5a, 5b clearly show that an initial formation of hexagonal C-rings is more preferable than pentagons. At the same time, gradual growth of quasi-graphene island and its further swelling, due to appearance of aside pentagons (Fig. 5f), make the binding energies of semi-fullerenes, containing carbon pentagons or hexagons in the center, even more. After achieving certain diameter of semi-fullerene embryo, their further growth continues as CNT growth [13, 16]. In the case of a smooth Ni(111) substrate, this critical diameter is about 0.8-0.9 nm. Figs. 5e, 5f show appearance of capped CNTs with *zz*- and *ac*-chiralities, respectively. Since the number of C atoms directly contacting the substrate are limited by circles in the latter configurations, their E_{bind} values noticeable decrease.

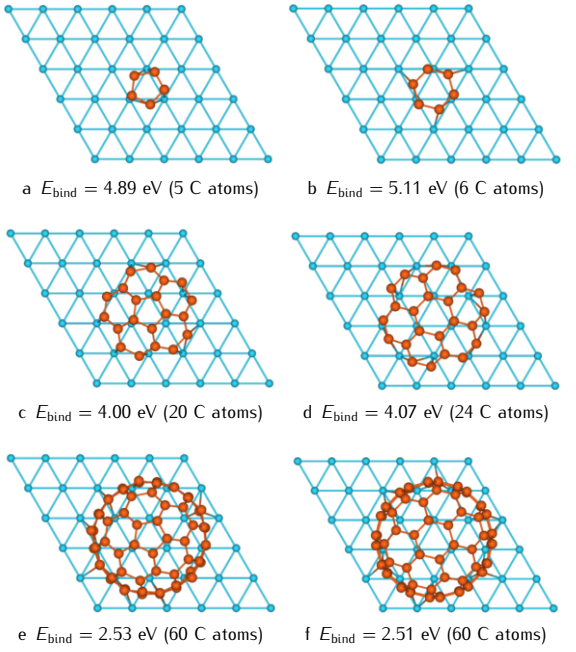

Figure 5. Models of capped CNT embryos growth upon 6×6 surface supercell of smooth Ni(111) slab (only external substrate layer is shown), beginning with appearance of 5-6 atom C-ring islands (a,b), their growth to quasi-graphene swelled flakes (c,d), up to creation of capped nanotubes with: zigzag- (e) or armchair- (f) chiralities (the rings of CNTs contacting to substrate are not visible here since their diameter is constant).

Since in the current study we have used 2D periodic models of CNT-Ni interconnects, they describe growth of SW CNT bundles containing nanotubes of identical chiralities not individual CNTs. Parameters of CNT bundles containing nanotubes of either *ac*- or *zz*-chiralities are shown in Fig. 6, they are comparable with those measured experimentally or simulated theoretically [2, 35].

In any case, appearance of carbon pentagons upon a smooth nickel (111) substrate demands a certain energy supply. On the other hand, a presence of Ni nanoclusters as well as other structural defects on the smooth substrate makes the growth of graphene monolayer unlikely since the curvature of carbon adlayer clearly means a presence of both hexagons and pentagons from C atoms. Thus, the nanostructured Ni(111) substrate is a good catalyst for

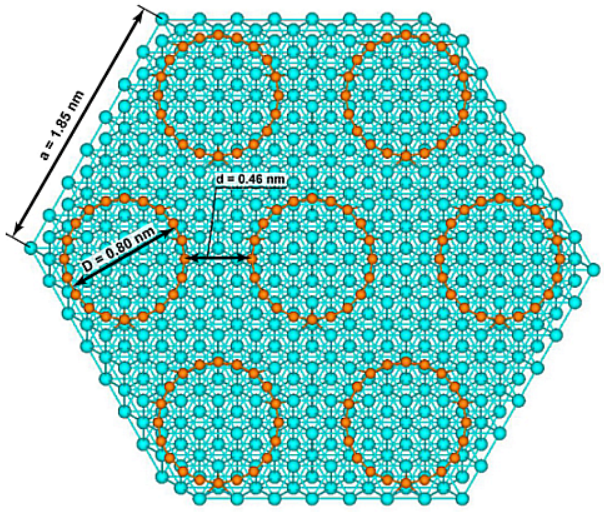

a

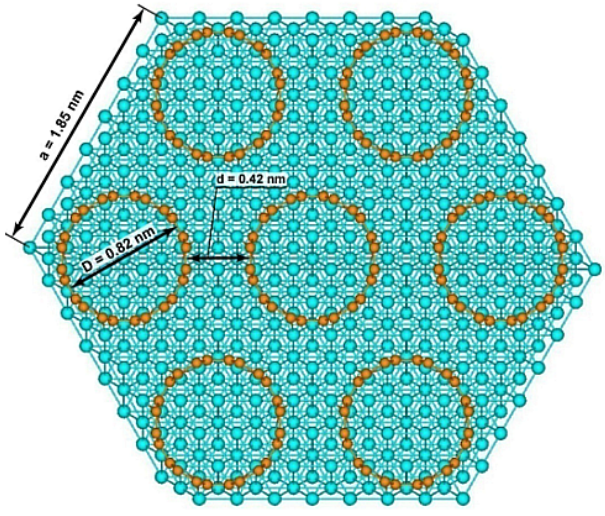

b

Figure 6. Bundle fragments and parameters of CNT-Ni(111) interconnect sections for *ac*-(6,6) (a) and *zz*-(10,0) (b) nanotube chiralities.

growth of both carbon nanotubes and fullerenes. And the energies of bonding between CNTs growing on smooth and nanostructured Ni substrates differ substantially (Fig. 7), thus confirming noticeably larger stability of the latter CNT-Ni contacts.

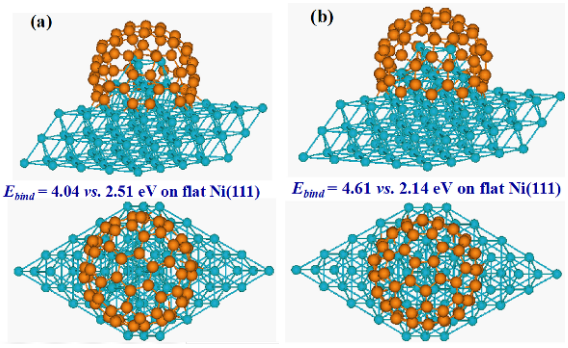

Figure 7. Side (upper) and top (lower) views of 2D 5×5 supercells demonstrating an initial stage of the CNT growth of either *ac*- (a) or *zz*- (b) type chirality upon the nanostructured Ni(111) surface.

3.5. Models of association of C atoms upon θ-Al_2O_3 substrate

We have also performed a large-scale simulation of the graphene (0001) monolayer positioned on the θ-Al_2O_3(110) surface employed to mimic a nanoporous wall of amorphous alumina membrane (Fig. 8). At the same time, supercell fragments of graphene (0001) nanosheets can be considered as both the outer walls of either multi-walled carbon nanotube or carbon nanoscroll (CNS) [36] with large diameter (~100 nm). The calculated energies of graphene adhesion in the absence and partial presence of atomic hydrogen after hydrocarbon dissociation allow us to characterize the interaction between the alumina membrane and modeled MW CNTs or CNSs.

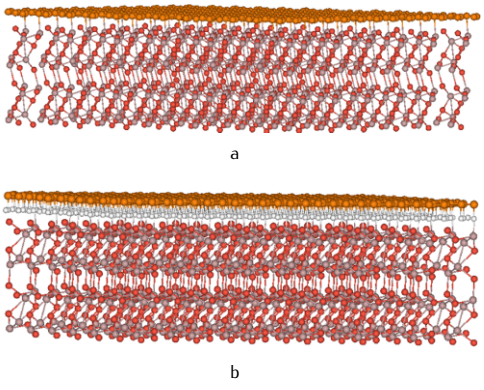

a

b

Figure 8. Side views for models of graphene (0001) sheet positioned atop θ-Al_2O_3(110) substrate (a), the same as (a) but in presence of the hydrogen monolayer in the interface between the graphene and θ-Al_2O_3(110).

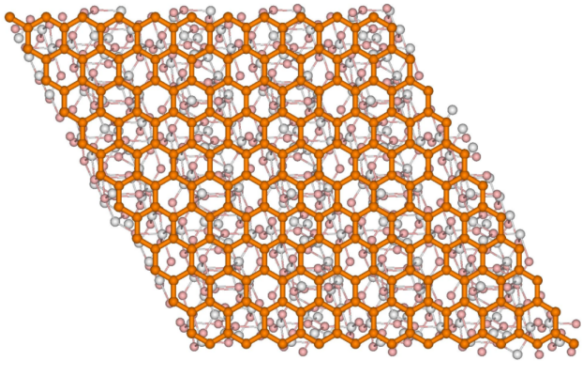

Figure 9. Top view for both models of graphene (0001) sheet positioned atop θ-Al_2O_3(110) substrate as shown in Fig. 8 (external hexagonal graphene monolayer is well-visible).

Although a structural compatibility between the quasi-graphene monolayer and the θ-alumina (110) substrate has been well-established (Fig. 9), the calculated value of binding energy for graphene positioned on the perfect θ-Al_2O_3(110) surface yields 0.40 eV *per* C atom (although the lattice mismatch between the adsorbent and adsorbate is rather negligible, it is five times smaller than the value for a single carbon atom on the θ-Al_2O_3(110) as present in Table 2), while insertion of hydrogen monolayer increases E_{bind} to 0.76 eV. From these results, we can conclude that the presence of hydrogen during the CVD growth of CNT inside alumina membrane plays an important role. Moreover, in this case, dissociation of C_mH_n molecules can be partial not total. Analysis of results obtained for the C/θ-Al_2O_3(110) interface clearly shows that in absence of metal catalysts (*e.g.*, Ni) on the bottom of the nanopores inside alumina membrane the carbon structures could grow rather from the walls towards the centers of nanopores: either carbon nanoscrolls and their bundles or thick MW CNTs and carbon nanofibres with rather amorphous morphology [37]. In any case, we predict the effectiveness of CNT growth from the surface of the nanostructured Ni or other metallic catalyst, which provides a higher stability of interconnects applied in nanoelectronics [1].

3.6. Electronic structure of SW CNTs grown on Ni substrates

A strong chemical bonding leads to the substantial electronic charge transfer and redistribution of the electronic density within the SW CNT-Ni interconnect. The values of charge transfer towards the nearest carbon atoms across the interfaces and interconnects are present in Table 3. In the case of interconnects between the *ac*-CNT bundle and smooth Ni(111) substrate (Fig. 6), the interfacial C ring accepts the electronic charge 14.07 *e* (altogether 12 atoms). For *zz*-CNT/Ni(111) in the same model, the Ni substrate transfers to the contacting nanotube ring an electronic charge of 13.84 *e* (10 C atoms), the electron charge redistributions illustrate this (Fig. 10).

Table 3. Calculated charge, Δq (in e), transferred from Ni(111) substrate, modeled by slab with 5×5 supercell, to C nanostructures positioned atop it.

C/Ni(111) structure (with number of contacting carbon atoms)	Charge transfer to all adatoms contacted to Ni	Δq per C atom
zz-CNT atop smooth Ni(111) (10)	13.84	1.38
ac-CNT atop smooth Ni(111) (12)	14.07	1.17
ac-CNT atop nanostructured Ni(111) (12)	13.34	1.11
zz-CNT atop nanostructured Ni(111) (10)	10.14	1.01
Single C atop *hcp* site on Ni(111) (1)	0.97	0.97
C adlayer atop *hcp* sites on Ni(111) (25)	23.75	0.95
C atoms forming embryo atop Ni(111) (6)	3.93	0.65
Graphene (0001) sheet atop Ni(111) (50)	28.00	0.56

When comparing the electron charge redistributions in SW CNT of the same chirality grown from both smooth and nanostructured Ni substrates (*cf.* Figs. 10 and 11) we can observe essential differences between both series of plots which can be described by the noticeable influence of nickel nanocluster positioned upon the substrate (Fig. 1c). There are two important differences between them: (*i*) markedly larger difference of densities for planes crossing boundary carbon rings (the lower plots in both Figures) and (*ii*) if carbon rings above the Ni-CNT interconnect in the case of smooth substrate are characterized by the deficiency of electron density (especially *zz*-CNT, Fig. 10), all the carbon rings above the nanostructured substrate possess the enhanced electronic density particularly supplied by Ni nanocluster. As a result, the Mulliken charges of boundary C atoms above a smooth substrate are slightly larger than those above the cluster (Table 3) which can be explained by a particular electronic charge transfer from the higher C rings to the interconnect (Fig. 10). On the contrary, the markedly higher values of E_{bind} in the nanostructured Ni-CNT interconnects (Fig. 7) can be caused by considerably higher electronic density redistribution in them, *i.e.*, a more strong bonding.

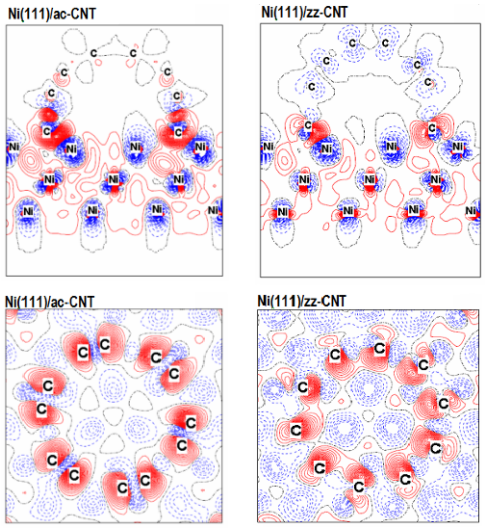

Figure 10. Charge redistributions between the bundles of *ac*-CNT (left plots) and *zz*-CNT (right plots) with the smooth Ni(111) substrate (the total density in the SW CNT-Ni interconnect minus the sum of electronic densities in separate SW CNT and nickel substrate). The cross-section planes are shown above while section planes crossing carbon atoms of contacting rings are positioned below: Black (dash-dot) isolines correspond to the zero level. Blue (dash) isolines stand for a decrease in the electron density while red (solid) lines for an increase. Isodensity curves are drawn from -0.05 to +0.05 e a.u.$^{-3}$ with an increment of 0.00167 e a.u.$^{-3}$.

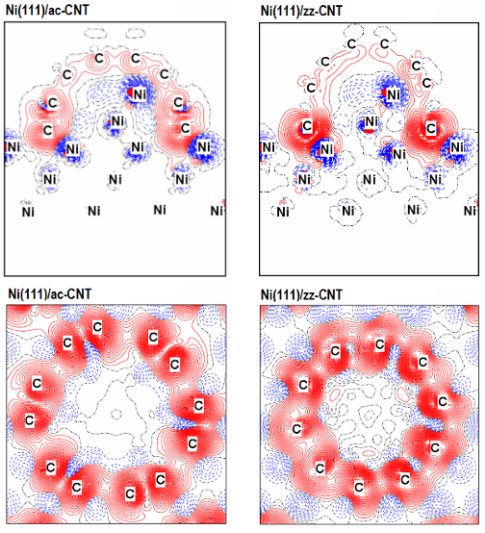

Figure 11. Charge re-distributions between the bundles of *ac*-CNT (left plots) and *zz*-CNT (right plots) with the nanostructured Ni(111) substrate. Details of plots are the same as in Fig. 10.

Upper parts of both Figs. 10 and 11 clearly show a more homogeneous redistribution of the electronic density along the carbon nanotube with *ac*-chirality (including its semi-fullerene cap) which is well-known as a conducting nanostructure, unlike the semiconducting *zz*-CNT [35]. Lower part of Fig. 11 indicates on the possible conductivity between adjacent *ac*-CNTs within the bundle.

The calculated DOSs presented in both Figs. 12 and 13 also confirm the larger reactivity of the nanostructured Ni(111)/CNTs interconnects as compared to the interconnects on a smooth Ni(111) substrate, due to a larger shift of bands and change of their morphologies. In any case, the projected DOS for both CNT/Ni structures explicitly shows hybridization of Ni 3*d* and C 2*p* orbitals.

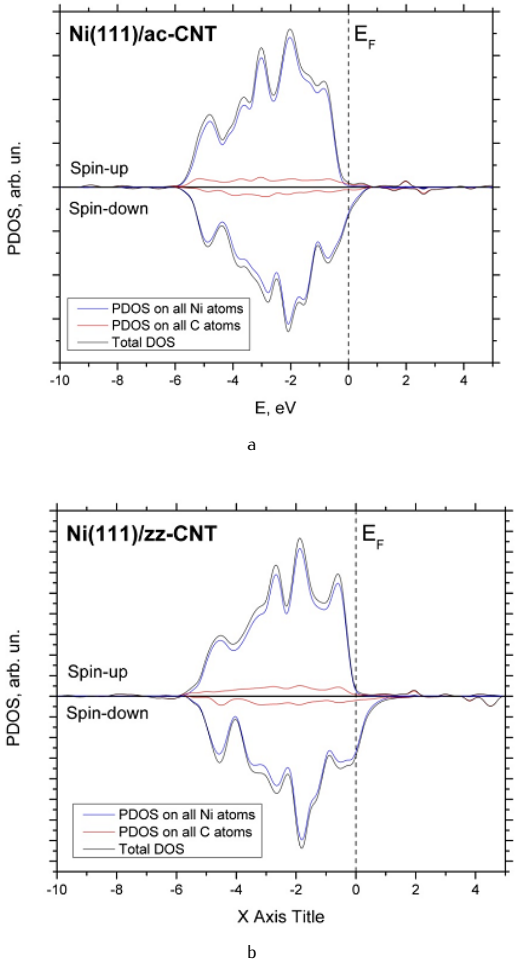

Figure 12. The one-electron density states of the smooth Ni(111) interconnects with the bundles of *ac*- and *zz*-CNTs (a and b, respectively).

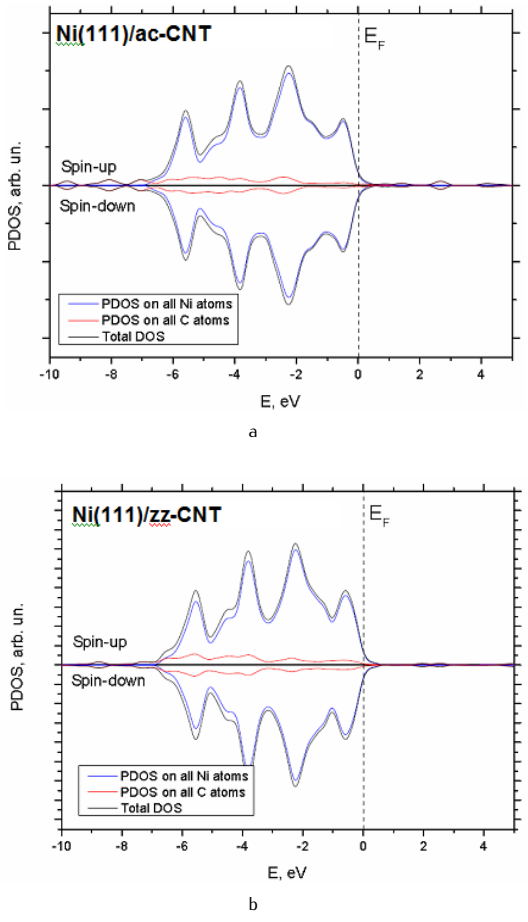

Figure 13. The one-electron density states of the nanostructured Ni(111) interconnects with the bundles of *ac*- and *zz*-CNTs (a and b, respectively).

4. Conclusions

We have developed the 2D models of CNT bundle growth on both smooth and nanostructured Ni(111) as well as θ-Al_2O_3 catalyst substrates. For these simulations a series of large-scale DFT-LCAO calculations using the *CRYSTAL-06* code have been performed[2]. Results obtained allow us to predict quite effective and reproducible mechanism for the growth of carbon nanotubes upon the nanostructured Ni(111) substrate. The driving force of CNT growth upon the catalyst surface (when using a CVD method providing a permanent flow of hydrocarbon molecules towards the substrate) has been found to be the formation of C-pentagons within the graphene islands, which then swell, forming quasi-fullerene embryos upon the surface. They appear as a result of dissociation of the hydrocarbon molecules moving towards the catalyst substrate. If on the smooth catalytic substrate, the formation of C-pentagons within the graphene monolayer island demands a certain energy supply, then on a nanostructured nickel (111) substrate, growth of C_n islands with a mixed hexagon-pentagon morphology occurs spontaneously and results in a formation of semi-fullerenes and capped CNTs grown on the nanostructured Ni(111) substrate. Simulations on the electronic properties of CNTs grown on the Ni substrate confirm the decisive role of Ni nanoclusters in strengthening the Ni-CNT interconnects. Analysis of these properties has allowed us to clarify a reason for noticeable differences between the *ac*- and *zz*-CNTs.

In the absence of metal catalyst nanoclusters on the bottom of the nanopores inside alumina membrane the carbon structures can grow from the walls towards the centers of nanopores: either in the form of carbon nanoscrolls or rather thick amorphous microtubes. Moreover, when applying the CVD method for growth of carbon nanostructures, the dissociation of C_mH_n molecules upon alumina substrate can be partial, not total, due to the formation of H-bonds with oxygen atoms of alumina surface and its further hydroxylation.

At the bottom level of the multiscale modeling, *ab initio* methods can be used for determining the electronic structure of the assumed carbon-metal nanocomposites. Moreover, the obtained results can be employed for construction of single-particle Hamiltonian used in the analytical tight-binding calculations of the conducting channels in the Me/MW-CNT interconnects, as well as in further MD and KMC simulations.

Acknowledgments

This study has been supported by EC FP7 CATHERINE Project. S.P. is thankful for the financial support through ESF project Nr. 2009/0216/1DP/1.1.1.2.0/09/APIA/VIAA/044. Authors are grateful to Prof. R.A. Evarestov for stimulating discussions.

References

[1] M. Ahlskog, Ch. Laurent, M. Baxendale, M. Huhtala, In: H.S. Nalwa (Ed.), Encyclopedia of Nanoscience

[2] R. Dovesi et al., CRYSTAL06 User's Manual (University of Torino, Turin, 2006), http://www.crystal.unito.it/

and Nanotechnology Vol. 3 (American Sci. Publishers, Valencia, CA, 2004) 139
[2] A. Loiseau et al., C. R. Phys. 4, 975 (2003)
[3] H. Zhu et al., Small 1, 1180 (2005)
[4] S. Hofmann et al., Nano Lett. 7, 602 (2007)
[5] H. Amara, J.-M. Roussel, C. Bichara, J.-P. Gaspard, F. Ducastelle, Phys. Rev. B 79, 014109 (2009)
[6] C. Journet et al., Nature 388, 756 (1997)
[7] J. Gavillet et al., Phys. Rev. Lett. 87, 275504 (2001)
[8] J. Gavillet et al., J. Nanosci. Nanotechno. 4, 346 (2004)
[9] J.-F. Colomer et al., Chem. Commun. 14, 1343 (1999)
[10] A.G. Nasibulin, P.V. Pikhitsa, H. Jiang, E.I. Kauppinen, Carbon 43, 2251 (2005)
[11] M. Lin et al., Nano Lett. 6, 449 (2006)
[12] H. Amara, C. Bichara, F. Ducastelle, Phys. Rev. Lett. 100, 056105 (2008)
[13] N.I. Alekseev, N.A. Charykov, Russ. J. Phys. Chem. A 82, 2191 (2008)
[14] F. Ding, K. Bolton, A. Rosén, J. Phys. Chem. B 108, 17369 (2004)
[15] F. Ding et al., Nano Lett. 8, 463 (2008)
[16] O.V. Yazyev, A. Pasquarello, Phys. Rev. Lett. 100, 156102 (2008)
[17] A. Börjesson, W. Zhu, H. Amara, C. Bichara, K. Bolton, Nano Lett. 9, 1117 (2009)
[18] Q.M. Zhang, J.C. Wells, X.G. Gong, Z. Zhang, Phys. Rev. B 69, 205413 (2004)
[19] S. Reich, L. Li, J. Robertson, Phys. Rev. B 72, 165423 (2005)
[20] M. Cantoro et al., Nano Lett. 6, 1107 (2006)
[21] V.L. Kuznetsov, A.N. Usoltseva, A.L. Chuvilin, E.D. Obraztsova, J.-M. Bonard, Phys. Rev. B 64, 235401 (2001)
[22] J. Zhao, A. Martinez-Limia, P.B. Balbuena, Nanotechnology 16, S575 (2005)
[23] Y.-A. Zhu, Y.-C. Dai, D. Chen, W.-K. Yuan, Surf. Sci. 601, 1319 (2007)
[24] S. Piskunov, G. Zvejnieks, Yu.F. Zhukovskii, S. Bellucci, Thin Solid Films (in press)
[25] Yu.F. Zhukovskii, E.A. Kotomin, B. Herschend, K. Hermansson, P.W.M. Jacobs, Surf. Sci. 513, 343 (2002)
[26] Yu.F. Zhukovskii, N. Pugno, A.I. Popov, C. Balasubramanian, S. Bellucci, J. Phys.: Condens. Matter 19, 395021 (2007)
[27] Yu.F. Zhukovskii, S. Bellucci, S. Piskunov, L. Trinkler, B. Berzina, Eur. Phys. J. B 67, 519 (2009)
[28] J.P. Perdew, K. Burke, M. Ernzerhof, Phys. Rev. Lett. 77, 3865 (1996)
[29] H.J. Monkhorst, J.D. Pack, Phys. Rev. B 13, 5188 (1976)
[30] H.-S. Kim, S.A. Zygmunt, P.C. Stair, P. Zapol, L.A. Curtiss, J. Phys. Chem. C 113, 8836 (2009)
[31] S.P. Adiga, P. Zapol, L.A. Curtiss, Phys. Rev. B 74, 064204 (2006)
[32] R.I. Duchovic, W.L. Hase, H.B. Schlegel, M.J. Frisch, K. Raghavachari, Chem. Phys. Lett. 89, 120 (1982)
[33] G. Kalibaeva et al., J. Phys. Chem. B 110, 3638 (2006)
[34] M. Fujita, R. Saito, G. Dresselhaus, M.S. Dresselhaus, Phys. Rev. B 45, 13834 (1992)
[35] J-C. Charlier, X. Blase, S. Roche, Rev. Mod. Phys. 79, 677 (2007)
[36] O. Zhou et al., Science 263, 1744 (1994)
[37] P. Ciambelli, D. Sannino, M. Sarno, A. Fonseca, J.B. Nagy, J. Nanosci. Nanotechno. 4, 779 (2004)